DC-link Voltage Control of a Full Power Converter for Wind Generator Operating in Weak-Grid Systems

Xibo Yuan, *Student Member, IEEE*, Fei (Fred) Wang, *Senior Member, IEEE*, Dushan Boroyevich, *Fellow, IEEE*, Yongdong Li, *Member, IEEE*, and Rolando Burgos, *Member, IEEE*

***Abstract*—When the wind power accounts for a large portion of the grid power, it may need to help the grid voltage and frequency regulation. This paper investigates a permanent-magnet wind generator with a full power voltage-source converter in weak-grid mode, where the dc-link voltage needs to be controlled from the generator side instead of the grid side. The energy relationship of the wind generator, dc-link energy storage, and load is established. An intrinsic right-half-plane zero, together with the wind power characteristics, the mechanical system inertia, and the dc-link energy storage, is identified as the physical limitations for the control. With the understanding of the system energy relationship and limitations, a hybrid adaptive control algorithm is proposed that searches for the optimal generator acceleration to achieve the maximum wind generator power change rate to match the load power variation. The proposed control scheme is verified through simulation of a 1.5-MW wind system as well as through the experiment of a scaled 1-kW, DSP-/field-programmable-gate-array-controlled, permanent-magnet-generator-based test bed. The results show that it is feasible to regulate dc link by the generator-side converter through the generator speed control. Some important applications issues are also investigated, including the dc-link energy storage requirement, wind speed change impact, and control transition between the weak-grid and strong-grid modes.**

***Index Terms*—Permanent-magnet generator (PMG), voltage control, weak grid, wind power.**

I. Introduction

TODAY, while most wind power is transferred to the grid via variable-speed doubly fed induction generators in large wind turbines, the permanent-magnet generator (PMG) interfaced to the grid through a full power converter is being increasingly adopted due to its higher power density and better controllability, especially so during grid faults [1]–[5]. Full power conversion schemes can use various popular ac–ac converter topologies [6]–[8]. Fig. 1 shows a typical full power wind converter based on the back-to-back two-level voltage-source converter (VSC) topology. In normal grid-connected operation, when wind power is relatively a small portion of a strong grid, the grid-side converter is used to regulate the dc-link voltage while the generator-side converter regulates the PMG speed to achieve the desired power transfer under a given wind condition [9]–[16]. This is normally achieved following the maximum power point tracking (MPPT) scheme [17]–[20].

On the other hand, in the case of operating in a weak grid, when wind power becomes a significant portion of the power system or even the sole energy source, the wind power generator and its converter are expected to help maintain the grid-side voltage and frequency. The weak-grid condition can be a result of intentional separation or islanding from the grid, or grid faults (unintentional islanding). It applies as well to the stand-alone operating mode. In such cases, the grid-side converter operates as an inverter regulating the grid-side voltage and frequency, while the dc-link voltage should be naturally controlled from the generator side. The basic principle is that the generator-side converter should try to adjust the generator output power to balance the load power need, such that the dc-link voltage can be maintained. Given the variable speed and the nonlinear power characteristics of the wind turbine, the dc-link control is a significant challenge under this condition. In low-power wind generator systems, for instance, a resistor with chopping control is used to burn the excess energy on the dc link during strong transients [19], [20], which is a solution neither practical nor acceptable for high-power applications.

As mentioned before, the control of the grid-connected mode is well studied. The transition algorithm from the grid-connected mode to islanding mode or weak-grid mode, including the detection schemes for grid faults or islanding conditions, has also been studied in several papers [21], [22]. Consequently, this paper will focus on the control of PMG in weak-grid mode (including islanding and stand-alone mode) for wind applications interfaced through a back-to-back three-phase VSC, as shown in Fig. 1. The grid-side converter operation as an inverter is also well known, provided that the dc-link voltage is well regulated. Therefore, this paper specifically focuses on dc-link voltage regulation using the generator-side converter with the generator speed as the control lever.

Section II of this paper presents the control methodology for the dc-link voltage by controlling the PMG speed through the generator-side converter. The energy relationship of wind turbine, PMG, dc-link capacitor, and load is established. An intrinsic right-half-plane zero (RHZ), together with the wind

Manuscript received May 19, 2008; revised October 29, 2008 and February 11, 2009. Current version published August 28, 2009. This work was supported under a supplemental grant for research outreach from the National Science Foundation under Award EEC-9731677. This paper was presented at the Applied Power Electronics Conference and Exposition (APEC), February 24–28, 2008, Austin, TX. Recommended for publication by Associate Editor Z. Chen.

X. Yuan is with the Center for Power Electronics Systems, Virginia Polytechnic Institute and State University, Blacksburg, VA 24061 USA, and also with the National Key Laboratory of Power Systems, Department of Electrical Engineering, Tsinghua University, Beijing 100084, China (e-mail: yuanxb05@mails.tsinghua.edu.cn).

F. Wang, D. Boroyevich, and R. Burgos are with the Center for Power Electronics Systems, Virginia Polytechnic Institute and State University, Blacksburg, VA 24061 USA (e-mail: wangfred@vt.edu; dushan@vt.edu; rolando.burgos@us.abb.com).

Y. Li is with the National Key Laboratory of Power Systems, Department of Electrical Engineering, Tsinghua University, Beijing 100084, China (e-mail: liyd@mail.tsinghua.edu.cn).

Digital Object Identifier 10.1109/TPEL.2009.2022082

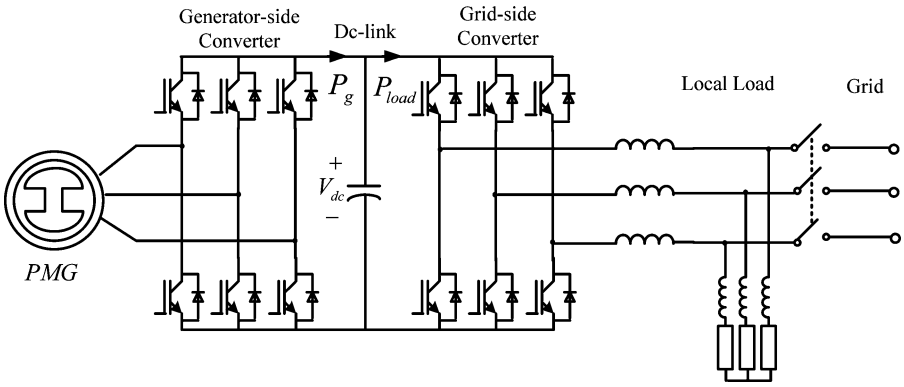

Fig. 1. PMG-based wind system with full power VSC.

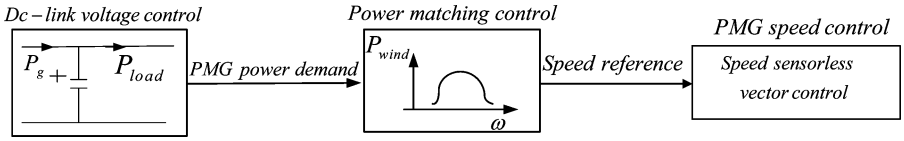

Fig. 2. Basic dc-link voltage control scheme.

power characteristics, the mechanical system inertia, and the dc-link energy storage, is identified as the physical limitations for the control. A hybrid adaptive control algorithm is proposed that searches for the optimal PMG acceleration to achieve the maximum PMG power change rate to match the load power variation. Section III provides control method verification through simulation and experiments. The simulation is carried out in MATLAB for a 1.5-MW wind power system, while a scaled 1-kW, DSP/field-programmable gate array (FPGA) controlled, PMG-based test bed is used for the experimental verification. Some of the key application issues for the proposed control method are studied and discussed in Sections II and IV, including the dc-link energy storage/capacitor requirement, wind speed change impact, control transition between the weak-grid and MPPT modes, and coordination with pitch angle control.

II. Proposed Control Method

A. Basic Control Principle and Requirements

The basic control principle is illustrated in Fig. 2. As can be seen in Fig. 2, in order to maintain the dc-link voltage, the generator output power P_g should track the load power demand $P_{\rm load}$, which can be achieved through controlling the generator speed based on the power–speed characteristics of the wind turbine. Fig. 3 shows the power–speed characteristic of a 1.5-MW turbine generator at different wind speeds [25]. Each of the curves in Fig. 3 has two sectors (I and II) with positive and negative slopes, respectively. For a given power level, there can be two possible operating points (e.g., B_1 and B_2 in Fig. 3) corresponding to sectors I and II, respectively, and the actual operating point can be determined by comparing the PMG power variation with respect to speed change [20]. In addition to the turbine/generator speed, the wind turbine pitch angle can also be controlled to regulate the wind power. In this paper, the pitch angle is first assumed to be fixed at 0° for the simplicity of analysis, and a discussion is provided later on how to incorporate the pitch angle control in the proposed control scheme.

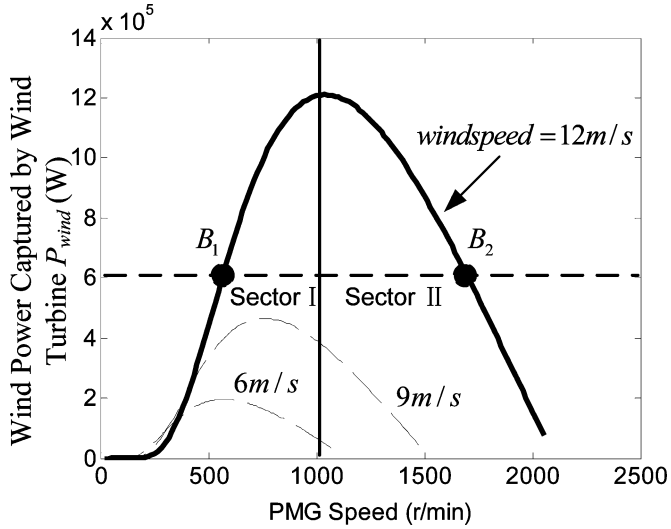

Fig. 3. Wind power–speed characteristics for a 1.5-MW system [25] (air density $\rho = 1.29$ kg/m^3, turbine swept area $A = 3215\,\mathrm{m}^2$, maximum power coefficient $C_{p\max} = 0.4$, and gear ratio 50).

In order to develop a robust control scheme, we will first establish the relationship between turbine/PMG speed, dc-link voltage, and system parameters. The amount of wind power captured by the wind turbine $P_{\rm wind}$ can be expressed as in (1) [24], where ρ is the air density, A is the wind turbine swept area, v is the wind speed, and C_p is the power coefficient of the wind turbine and a function of the turbine (or generator) speed ω. For a given wind speed, $C_p(\omega)$ function has the same shape as shown in Fig. 3 with a maximum power coefficient $C_{p\max}$ corresponding to an optimal generator speed ω. Note that the generator speed has a fixed relationship with the turbine speed,

either equal for a direct drive or through the gear ratio when there is a gearbox. In this paper, the generator speed ω is used for both the generator and turbine speed assuming the gear ratio has been considered

$$P_{\rm wind} = \frac{1}{2}\rho {\rm A} C_p(\omega) v^3. \tag{1}$$

Neglecting the power converter losses, the dynamic equation of the dc-link voltage can be written as in (2), where $V_{\rm dc}$ and $i_{\rm dc}$ are the voltage and current of the dc-link capacitor, respectively

$$P_g - P_{\rm load} = V_{\rm dc} i_{\rm dc} = V_{\rm dc} C \frac{dV_{\rm dc}}{dt}. \tag{2}$$

Practically, P_g is equal to $P_{\rm wind}$ at steady state without considering losses. During PMG speed change, P_g differs with $P_{\rm wind}$ by the required mechanical power for acceleration or deceleration, as shown in (3), where J is the system inertia and generator losses (electrical and mechanical) are neglected

$$P_{\rm wind} - P_g = \omega J \frac{d\omega}{dt}. \tag{3}$$

From (2) and (3), it is clear that one option to control the dc-link voltage is to change the generator output power P_g (thus $P_{\rm wind}$) by controlling the generator speed. In order to obtain the relationship between the dc-link voltage $V_{\rm dc}$ and the generator speed ω, (1)–(3) can be combined to yield the following equation:

$$\frac{1}{2}\rho {\rm A} C_p(\omega) v^3 - P_{\rm load} - V_{\rm dc} C \frac{dV_{\rm dc}}{dt} = J\omega \frac{d\omega}{dt}. \tag{4}$$

Equation (4) shows the nonlinear relationship between the dc-link voltage and PMG speed due to the nonlinear $C_p(\omega)$ and the two second-order terms. Considering $P_{\rm load}$ as the disturbance, (4) can be linearized at a given operating point (e.g., dc-link voltage $V_{\rm dc0}$, PMG speed ω_0, and wind speed v_0). The transfer function of the dc-link voltage $V_{\rm dc}(s)$ and generator speed $\omega(s)$ is then described by the frequency-domain model in (5), where k is the slope of the curve in Fig. 3 corresponding to the operating point

$$\frac{V_{\rm dc}(s)}{\omega(s)} = \frac{k - J\omega_0 s}{V_{\rm dc0} C s} = \frac{J\omega_0}{V_{\rm dc0} C} \frac{(-s + (k/J\omega_0))}{s}. \tag{5}$$

As can be seen in Fig. 3, if the generator is operating in sector I, then $k > 0$ and the system will have an RHZ. This RHZ will add control complexity and limit the system performance. On the other hand, in sector II, $k < 0$ and the transfer function will have a left-half-plane zero (LHZ), which tends to be easier to deal with in control design. For a given power level, the PMG can operate at two speed points in sector I or II, as seen in Fig. 3. While it may be preferable to operate the turbine/generator in a particular sector for a particular application requirement (e.g., sector I for lower speed—thus lower mechanical loss and stress; sector II for higher stored kinetic energy capability), the control design ought to consider both sectors as the operating point can jump from one sector to the other during a fast wind speed or load change [25], [26]. Given the presence of the RHZ and other complexities associated with sector I, this paper will mainly focus on controller design for sector I. The design for sector II can follow the same procedure. The controller performance in both sectors is verified, and some results are presented in Sections III and IV. The difference between these two sectors regarding the control and mechanical power flow will also be discussed.

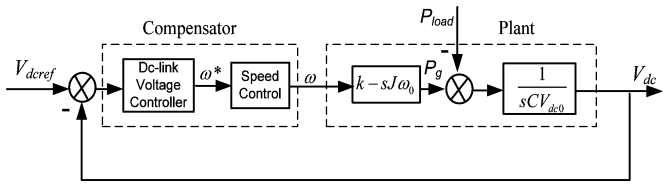

Fig. 4. DC-link voltage control block diagram.

Based on the aforementioned analysis, the dc-link voltage control during the weak-grid condition can be realized through the basic controller structure in Fig. 4. A dc-link voltage control loop can be used to generate the required PMG speed reference $\omega*$. The speed control can be implemented similarly as PMG control in the normal strong-grid-connected case [9]. By changing the generator speed ω, the wind power $P_{\rm wind}$ will change according to Fig. 3 ($P_{\rm wind} - \omega$ curves), and P_g will change with $P_{\rm wind}$ via (3) to compensate for the load power change, thus keeping the dc-link capacitor voltage regulated.

The dc-link voltage controller design must consider the performance requirements. There are two key performance parameters for the voltage regulation.

1) *DC-link voltage variation range*—The dc-link voltage dip or rise during the load power increase or decrease should be limited to the minimum voltage $V_{\rm dcmin}$ and maximum voltage $V_{\rm dcmax}$, respectively. $V_{\rm dcmin}$ setting should meet the grid-side ac voltage amplitude requirement, and $V_{\rm dcmax}$ cannot exceed the voltage ratings of the power semiconductor devices and dc-link capacitors. Equation (6) shows the constraints on $V_{\rm dcmin}$ and $V_{\rm dcmax}$, where $V_{\rm dc}$ is the dc-link voltage, $M_{\rm max}$ is the maximum modulation index, $V_{\rm line}$ is the grid-side ac line voltage magnitude, and $V_{\rm cap,device}$ is the maximum allowed voltage for dc-link capacitors and devices. Note that for a given application, $V_{\rm dcmin}$ and $V_{\rm dcmax}$ selections may need to consider other constraints, such as inrush conditions. This paper only considers relationships in

$$\begin{aligned} V_{\rm dc\,min} M_{\rm max} &> \sqrt{2} V_{\rm line} \\ V_{\rm dcmax} &< V_{\rm cap,device}. \end{aligned} \tag{6}$$

2) *DC-link voltage recovery time*—It is generally desirable to have fast response. This paper will use recovery time as a metric for performance comparison without imposing specific values.

B. Control Performance Analysis and Limits

A simple proportional–integral (PI) regulator can be used for implementing the dc-link voltage controller in Fig. 4. We use the same 1.5-MW system as depicted in Fig. 3, which operates in sector I, as an example. The PMG and converter system parameters are given in Table I with $C = 300$ mF, $V_{\rm dc0} = 700$ V, $J = 156.8$ kg·m^2, $v_o = 12$ m/s, at the operating point

TABLE I
PMG AND CONVERTER PARAMETERS OF A SAMPLE SYSTEM

Rated Power	1.5 MW	Rated PMG Voltage	460 V
Rated PMG Current	1883 A	Rated PMG Speed	1650 RPM (173 rad/s)
Rated Wind Speed	13 m/s	Number of PMG Poles	8
Wind Turbine System Inertia (Considering Gear Box Ratio)	156.8 kgm^2	Rated VSC Dc-link Voltage	700 V
Gear Box Ratio	1:50	VSC Dc-link Capacitance	300 mF
D-axis Inductance L_d	0.514 mH	Q-axis Inductance L_q	0.186 mH
Rated Frequency f	110 Hz	Stator Resistance R_s	0.514 mΩ

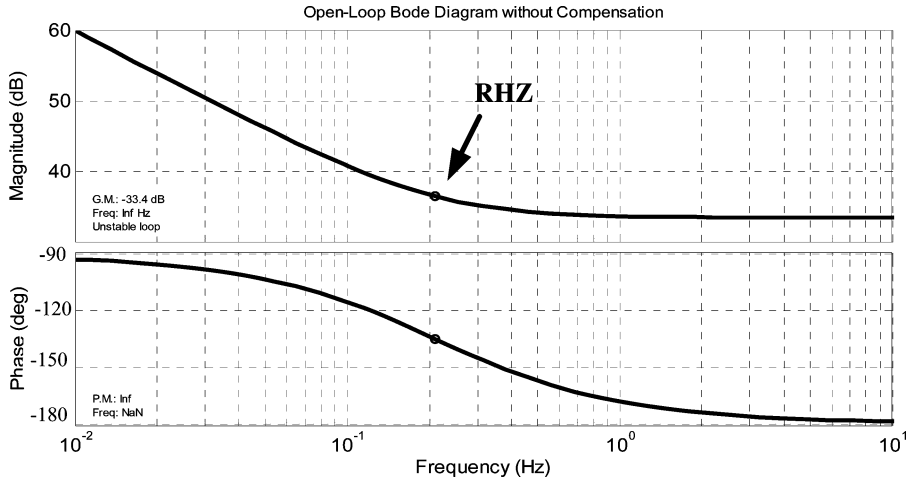

Fig. 5. Open-loop frequency response without compensator.

$P = 600$ kW, $\omega_0 = 62.8$ rad/s (sector I), $k = 13\,000$ N·m, and the corresponding RHZ is at 0.21 Hz. Fig. 5 shows the open-loop frequency response of the Fig. 4 system without the compensator. Since the crossover frequency can only be chosen below the RHZ to guarantee the system stability, the system performance with a simple PI regulator based on one operating point is limited.

In order to design an effective voltage regulator, it is important to understand the physical relationships of the dc-link voltage variation with load, wind turbine, PMG, and generator-side converter. It is also important to determine the physical limitations of the system during a load or wind condition change.

Consider the dc-link voltage dip phenomenon as a result of a step load increase. Assuming that $t = t_1$, the load power $P_{\rm load}$ increases by a step of $\Delta P_{\rm load}$ from an equilibrium point, as shown in Fig. 6, while the wind speed v stays unchanged. From the sector I wind power curve in Fig. 3, the generator speed should be increased such that more wind power can be captured to track the load power demand. During the acceleration, some of the wind power $P_{\rm wind}$ will convert to mechanical power $P_{\rm mec}$ corresponding to stored system kinetic energy due to the system inertia, which can be large for large wind turbines, and the

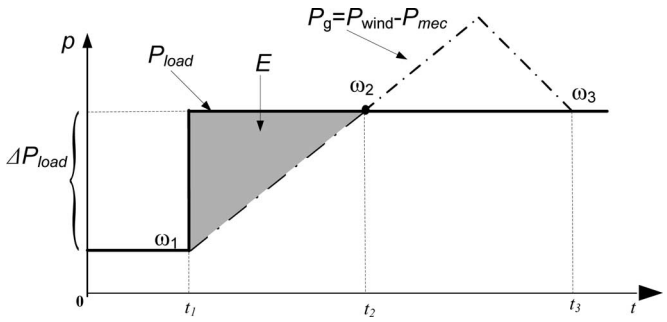

Fig. 6. DC-link voltage dips analysis (a constant $d\omega/dt$ assumed).

rest of $P_{\rm wind}$ will convert to PMG output power P_g (neglecting losses), which is, in turn, fed to the dc link through the generator-side converter. The system power flow during acceleration is illustrated in Fig. 7. From the power relationship, the PMG should not accelerate too fast when the wind turbine operates in sector I. Otherwise, much of $P_{\rm wind}$ may become $P_{\rm mec}$ due to high $d\omega/dt$, reducing available P_g, even if $P_{\rm wind}$ increases with ω in sector I.

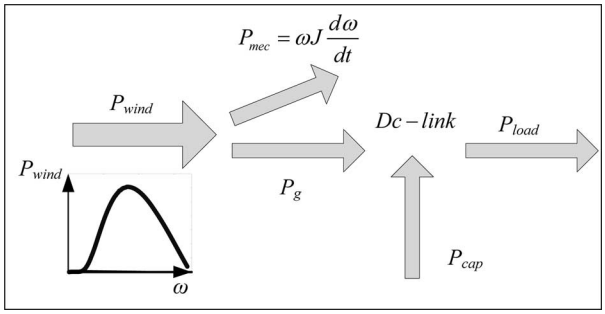

Fig. 7. System power flow during acceleration.

Therefore, there is a tradeoff between increasing $P_{\rm wind}$ and storing mechanical power $P_{\rm mec}$ by changing the generator speed for wind turbine working in sector I. There should be an "optimal" acceleration rate $d\omega/dt$ that can maximize P_g during a load increase. The shaded area in Fig. 6 denotes the energy that needs to be compensated by the dc-link capacitor owing to the P_g and $P_{\rm load}$ difference, thus resulting in the dc-link voltage dip. For a given capacitance value, the smaller the shaded area, the smaller the voltage drop will be. The shaded area can be minimized by maximizing the change rate of generator power P_g. To simplify the analysis, $dP_{\rm wind}/d\omega$ and acceleration $d\omega/dt$ are assumed to be constant, i.e., $dP_{\rm wind}/d\omega = k$ and $d\omega/dt = k_1$. The change rates of the wind power $P_{\rm wind}$ and the mechanical power $P_{\rm mec}$ can be expressed as (7a) and (7b), respectively. Their difference gives the generator output power P_g change rate as in (8)

$$\frac{dP_{\rm wind}}{dt} = \frac{dP_{\rm wind}}{d\omega}\frac{d\omega}{dt} = k\frac{d\omega}{dt} = kk_1 \tag{7a}$$

$$\frac{dP_{\rm mec}}{dt} = \frac{d(\omega J(d\omega/dt))}{dt} = k_1^2 J \tag{7b}$$

$$\frac{dP_g}{dt} = \frac{d(P_{\rm wind} - P_{\rm mec})}{dt} = kk_1 - k_1^2 J. \tag{8}$$

From (8), it can be seen that the maximum power change rate is determined by wind power–speed curve slope *k* and turbine generator inertia *J*. During a load increase, a sharper slope *k* corresponds to a faster power change rate, which will reduce the dc-link voltage drop and recovery time; on the other hand, a larger *J* will result in more stored kinetic energy during acceleration and less available energy to feed to dc link. By controlling the acceleration $d\omega/dt$ (assuming k_1 as constant in the analysis), a maximum dP_g/dt can be obtained for given *k* and *J*, as indicated in (8). For the sample system in Table I, the PMG output power change rate dP_g/dt with respect to PMG acceleration $d\omega/dt$ is plotted in Fig. 8 based on (8) with different *k* and *J*.

Clearly, dP_g/dt has a maximum $dP_{g(\max)}/dt$ corresponding to an optimal acceleration $d\omega/dt_{(\rm optimal)}$. Since the maximum dP_g/dt is desired for minimizing the dc-link voltage dip, the control should be designed to find the $d\omega/dt_{(\rm optimal)}$ that will lead to $dP_{g(\max)}/dt$. It should be pointed out that for any controller design, it is important to establish the physical limit to achieve the best possible regulation and dynamics. For example, the PMG torque control is limited by generator/converter voltage/current ratings and PMG inductance. From the aforementioned analysis, the key limits for the dc-link voltage control for the type of wind power system are *k* and *J*. Higher wind speeds indicate sharper slope *k* and larger $dP_{g(\max)}/dt$, as in Fig. 8(a). Lower inertia *J* corresponds to lower kinetic energy stored during acceleration, and therefore higher $dP_{g(\max)}/dt$, as in Fig. 8(b). This observation agrees with the system transfer function (5). The system performance in sector I is limited by RHZ, which is determined by *k* and *J*. The observation can also explain the response limitation of the wind system to the load increase under a given operating condition in sector I. In principle, higher available wind energy (i.e., higher wind speeds) should correspond to faster possible response to load change. However, the impact of inertia and generator/converter rating limits will also need to be considered. In general, lower wind speed, larger system inertia, and lower ratings will slow down the system response.

The aforementioned discussion applies directly to the load increase and voltage dip case in sector I. For the load decrease and voltage rise case in sector I, there should be an optimal deceleration rate $d\omega/dt$ that corresponds to a minimum dP_g/dt. Also note that for the wind generator working in sector II, $P_{\rm load}$ increase should trigger a speed decrease to increase $P_{\rm wind}$ and decrease $P_{\rm mec}$ at the same time. Therefore, the stored kinetic energy is released and converted to electrical energy, which helps to compensate for the load power increase and maintain the dc-link voltage. Consequently, in sector II, the system control bandwidth is not subject to the limit as in the case of sector I. The same discussion applies to load decrease and voltage rise as well.

C. Adaptive Controller

As explained before, the dc-link voltage controller in Fig. 4 should be designed such that the maximum dP_g/dt can be obtained dynamically. A simple PI regulator, with constant PI parameters based on a small-signal model for a given operating point, will achieve the desired performance only around this point. It cannot guarantee the maximum dP_g/dt dynamically during a large load change, and the control performance will deteriorate, thus causing larger dc-link voltage variation or longer recovery time. In order to optimize the system performance during large load change, a hybrid adaptive PI controller is proposed based on the power and energy relationship analysis described before.

The flowchart of the proposed hybrid adaptive dc-link voltage control is shown in Fig. 9. First, the sector for the operating point is determined as explained earlier [20]. In sector I, the control scheme is divided into two parts according to the error between measured and reference values of the dc-link voltage. When the error is within a certain range Δ, the PI controller parameters (proportional and integral gains K_p and K_i) are fixed, chosen with the values derived from the small-signal model to guarantee the steady-state performance. For example, for the operating point corresponding to Fig. 5 (sector I, $P = 600$ kW $\omega_0 = 62.8$ rad/s, $k = 13000$ N·m, and $v_o = 12$ m/s), a PI regulator with $K_p = 0.3$ and $K_i = 0.05$ can achieve a crossover

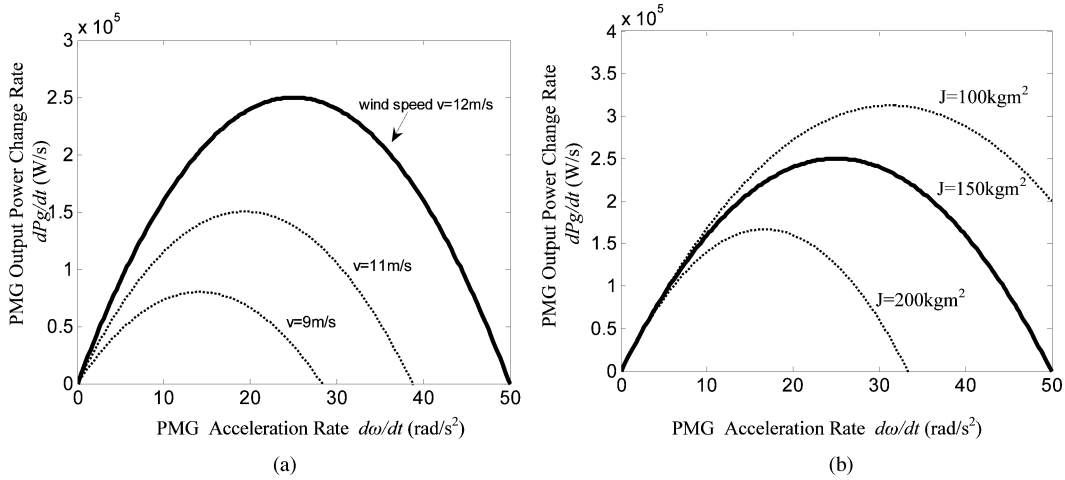

Fig. 8. PMG output power change rate with respect to acceleration rate. (a) With different wind speeds. (b) With different system inertia.

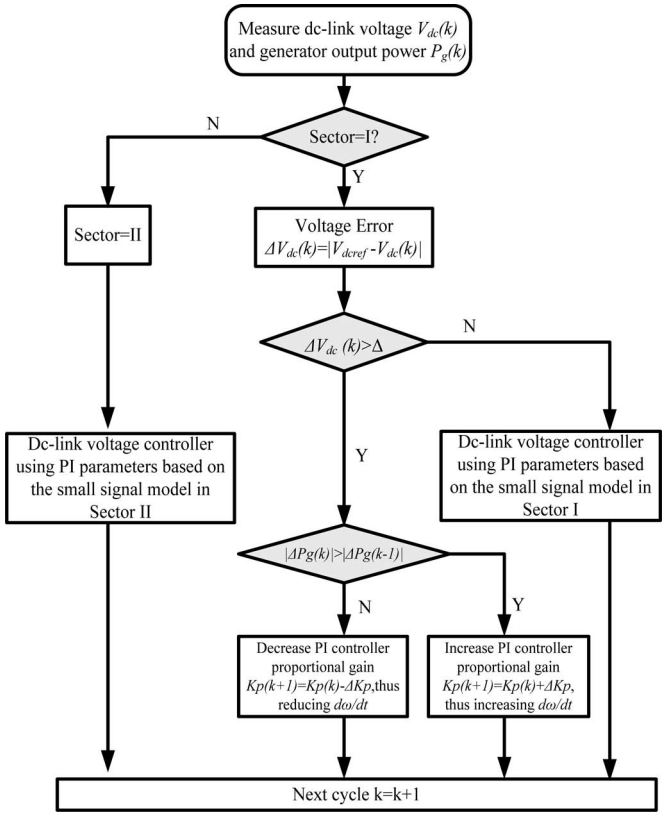

Fig. 9. Flowchart of the hybrid adaptive control method.

frequency of 0.04 Hz with a 72° phase margin. When the error exceeds Δ, the PI parameters are adapted to improve the dynamic response. Specifically, K_p is changed by a small increment of ΔK_p every control cycle to cause a change in PMG acceleration rate $d\omega/dt$. Note that the dc-link control cycle can be considerably longer than those of the inner speed/torque loops. When K_p is incremented, the proportional part of the dc-link voltage regulation will increase accordingly. Depending on the polarity of the voltage error, a larger or smaller speed reference $\omega*$ will result. For positive voltage error (voltage dip case), a larger $\omega*$ will cause the PMG speed to increase faster, i.e., larger $d\omega/dt$, through the speed/torque loop control; for negative voltage error (voltage rise case), a smaller $\omega*$ will cause the PMG speed to decrease faster, i.e., larger negative $d\omega/dt$. Both cases will make power change rate $|dP_g/dt|$ larger, which is desired for optimal dynamics as explained earlier. The increment of K_p will continue, until $|dP_g/dt|$ stops to increase, corresponding to the maximum power change rate and the optimal $d\omega/dt$. The power change rate $|dP_g/dt|$ can be measured and calculated through the converter output voltages and currents, as can be seen in (10), with a proper low-pass filter to suppress possible noise. If $|dP_g/dt|$ is observed to decrease, then decrease $|d\omega/dt|$ by decrementing K_p to find the new optimal point. When the voltage error becomes less than Δ, then K_p can return back to the original setting based on the small-signal model design.

For sector II operation, as explained earlier, the stored kinetic energy can help to compensate for the load change, and there exists no RHZ to limit system response. Therefore, a simple PI regulator with constant parameters can be used to achieve the desired performance. The bandwidth of the control can be higher than the sector I case, and limited only by the inner loops and system ratings.

For dc-link voltage regulation, the outer loop voltage controller needs to be used together with the inner speed controller, as shown in Fig. 4. In this paper, a sensorless speed control algorithm is adopted. The speed regulator with a vector-controlled torque regulator is shown in Fig. 10. The controller is based on the dynamic model of the PMG in the synchronous rotating frame (9), where $v_{sd}, v_{sq}, i_{sd}, i_{sq}$ are the PMG stator voltages and currents in d, q reference frame, L_d, L_q are the stator direct and quadrature axis inductances, R_s is the generator stator resistance, ω is the speed, and ψ is the rotor magnet flux linkage

$$v_{sd} = R_s i_{sd} + L_d \frac{di_{sd}}{dt} - L_q \omega i_{sq}$$
$$v_{sq} = R_s i_{sq} + L_q \frac{di_{sq}}{dt} + L_d \omega i_{sd} - \omega\psi. \quad (9)$$

In Fig. 10, the PMG torque is mainly controlled by the q-axis current component, while the d-axis current component is used

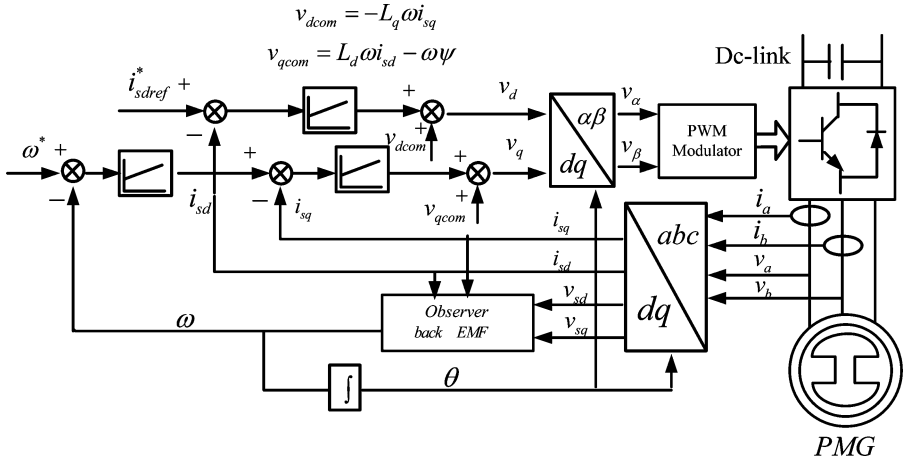

Fig. 10. Block diagram of the PMG speed and torque control [7], [25].

to achieve unity power factor, thus minimizing power losses and maximizing available torque [27]. A speed observer based on the PMG back electromotive force (EMF) is used to achieve speed sensorless control [28]. Since there is no "low-speed" operation for wind power application [29], the back-EMF-based observer can estimate the actual speed without problems. Neglecting converter losses, the generator and converter output power can be expressed as

$$P_g = \frac{3}{2}\left(v_{sd} i_{sd} + v_{sq} i_{sq}\right). \tag{10}$$

The design of the speed and torque/current regulators can follow the approach used in conventional PM motor drive design. Given the relatively slow dynamics for the dc-link controller, the speed and torque control does not have challenging dynamic requirements and can still be considered ideal in analyzing the energy relationship as done earlier.

D. Impact of DC-Link Energy Storage

As discussed before, the system response is limited by the wind power curve slope *k* and system inertia *J*, which determines the RHZ location. Large wind turbines/generators usually have large system inertia, and the system control bandwidth will be intrinsically limited. For the slow load power change within the system control bandwidth, the dc-link voltage can be well regulated by controlling wind generator speed and energy. Beyond that, the dc-link energy storage (in this case, capacitor) will need to handle the transient [30]. Therefore, the value of the three-phase converter dc-link capacitor will somewhat determine the magnitude of the voltage variation during fast load and source transients, e.g., load step increase. Using the same assumptions as in Fig. 6 for analysis, when the load power increases by $\Delta P_{\rm load}$ at time $t = t_1$, the generator output power P_g will increase with a change rate $k_2 = dP_g/dt$, as formulated in (8). Therefore, the generator output power can reach the load power within $T = (t_2 - t_1) = \Delta P_{\rm load}/k_2$. The voltage drop of the dc-link capacitor is the consequence of the energy difference between the generator output and the load (shaded area in Fig. 7), which can be expressed as E_c in (11). Combining (11) with stored capacitor energy relationship will yield (12)

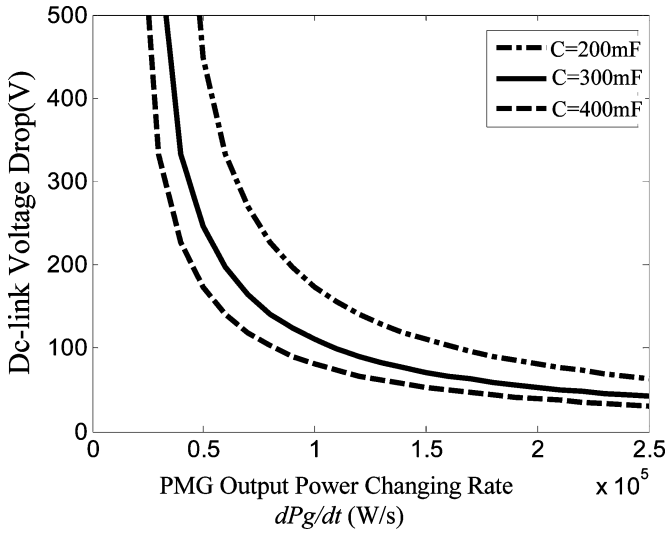

Fig. 11. DC-link voltage drop versus the capacitance value and PMG power change rate.

$$E_c = \frac{1}{2}\Delta P_{\rm load} T = \frac{1}{2}\frac{\Delta P_{\rm load}^2}{k_2} \tag{11}$$

$$\frac{1}{2}CV_{\rm dc}^2(t_1) - \frac{1}{2}CV_{\rm dc}^2(t_2) = \frac{1}{2}\frac{\Delta P_{\rm load}^2}{k_2}. \tag{12}$$

Given the requirement on dc-link voltage drop $V_{\rm dc}(t_1) - V_{\rm dc}(t_2)$ and $\Delta P_{\rm load}$, the capacitance value required can be found as

$$C = \frac{\Delta P_{\rm load}^2}{k_2\left(V_{\rm dc}^2(t_1) - V_{\rm dc}^2(t_2)\right)}. \tag{13}$$

Fig. 11 illustrates how the capacitance value and the PMG power change rate affect the dc-link voltage drop using the system in Table I under the condition of $\Delta P_{\rm load} = 300$ kW and initial $V_{\rm dc}(t_1) = 700$ V. Clearly, sufficient capacitors with proper capacitance and energy capability are needed to handle the transient load variation. The same conclusion can be drawn from the load power decrease and voltage rise case. The sample

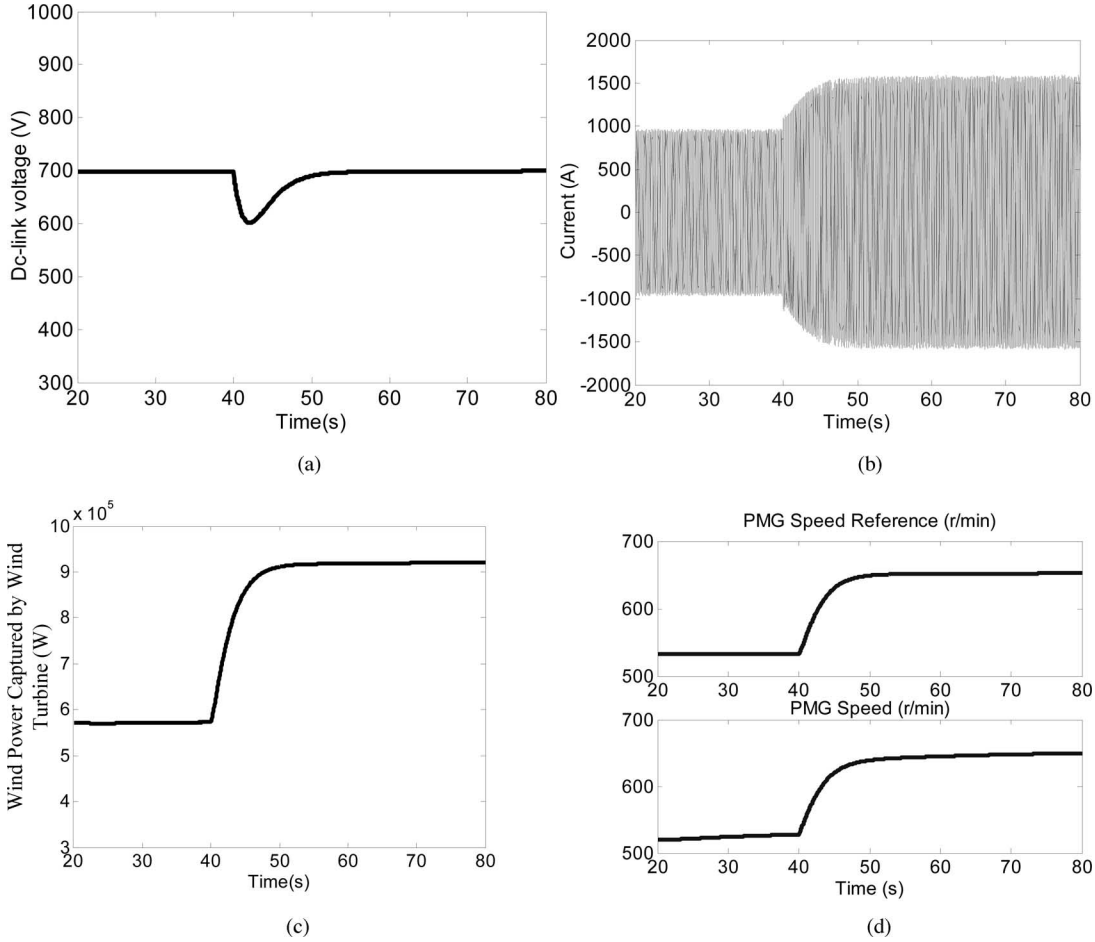

Fig. 12. Simulation results with a step load change under constant wind speed (12 m/s). (a) DC-link voltage. (b) PMG stator current. (c) Wind power captured by wind turbine. (d) PMG speed.

system in Table I uses $C = 300$ mF, and the expected voltage drop of 100 V for $dP_g/dt = 150$ kW/s has been verified through simulation.

Note that the dc-link capacitance values on the order of hundreds of millifarads, required for energy storage, seem to be excessive compared with the values used in other converter applications, e.g., industrial motor drives, for the same power rating. On the other hand, a 300-mF, 900-V capacitor bank used will have a size on the order of 0.18 m^3 based on commercial electrolytic capacitors, which is not unreasonable for a 1.5-MW converter. Increasing PMG and converter dc-link voltages can reduce the capacitance value but will not change the energy requirement, and therefore will not significantly change the capacitor size. However, slower load dynamics and more tolerable dc-link voltage will reduce the energy storage need. Of course, other energy storage means, such as battery and different capacitor technologies, may be considered more suitable for this application.

III. Simulation and Experimental Verification

A. Simulation Verification

The 1.5-MW wind power system described in Table I was modeled in MATLAB/Simulink to assess the proposed dc-link voltage control method. The simulated wind power–speed curves use the profiles in Fig. 3. A constant power load ranging from 0 to 1.5 MW is assumed on the dc link. The steady-state condition is the same as in Table I (sector I, $P = 600$ kW, $\omega_0 = 62.8$ rad/s, $k = 13\,000$, and $v_o = 12$ m/s). The compensated system crossover frequency is chosen as $f_0 = 0.04$ Hz to have a 72° phase margin. The corresponding proportional and integral gains for the PI regulator are 0.3 and 0.05, respectively. It should be pointed out that the margins on basic PI parameter settings are selected conservatively to accommodate the wide operating condition variations (wind speed, PMG speed, load, etc.). Their practical impact on the system dynamics due to large load variation is small with the adaptive controller. The dc-link voltage error threshold Δ for the adaptive controller is 5% (35 V). The speed and torque/current regulators have much higher bandwidth than the dc-link voltage regulator.

The dc-link voltage control algorithm is tested both in sectors I and II under load power step change and wind speed change. Some simulation results obtained are shown in Fig. 12 for constant wind speed of 12 m/s: (a) the dc-link voltage transient observed after applying a load step from 550 to 900 kW at time $t = 40$ s, with voltage effectively controlled at 700 V; (b) the phase current of the generator during this transient; (c) wind power P_{wind} change in response to the increased load power

TABLE II
SIMULATION RESULTS SUMMARY WITH 30% LOAD STEP AT DIFFERENT OPERATING POINTS

Wind Speed	8 m/s		10 m/s		12 m/s	
Performance	Voltage dip	Recovery time	Voltage dip	Recovery time	Voltage dip	Recovery time
Adaptive control	117 V	20 s	110 V	16 s	105 V	12 s
PI control	135 V	29 s	126 V	24 s	120 V	20 s

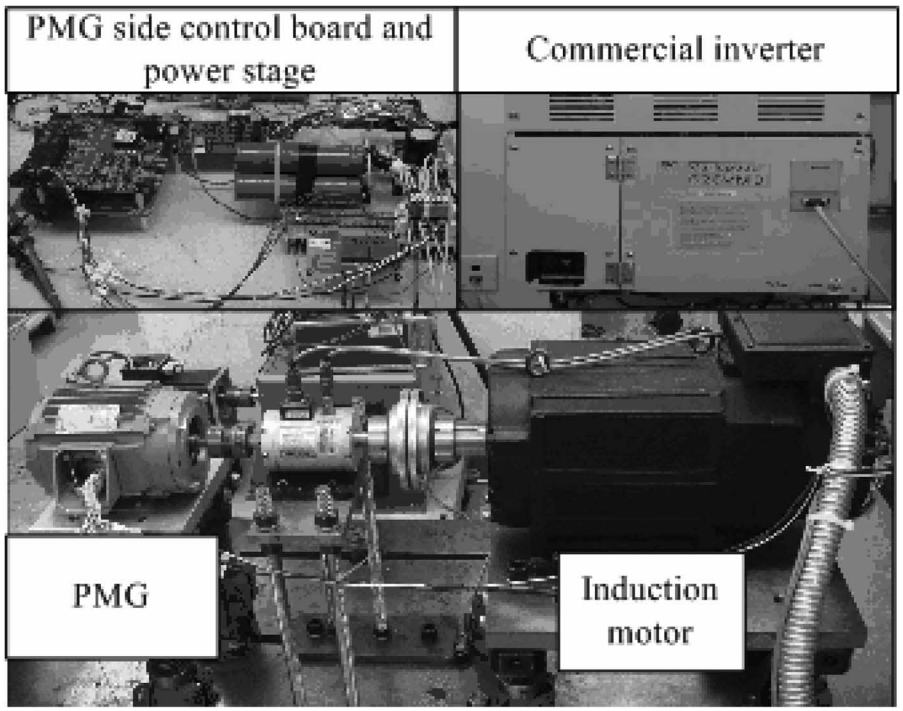

Fig. 13. Experimental setup.

demand; and (d) PMG speed reference and actual speed increase during the transient operation in sector I. It can be seen that the dc-link voltage is regulated well with an acceptable voltage dip, while the PMG is adjusting its speed to match the load power demand. Table II lists simulation result summary for several other wind conditions, all with the same controller setting. The control performs satisfactorily in all cases, with the adaptive control consistently outperforming the simple PI control.

The control is also tested through simulation for sector II operating point. For the same condition in Fig. 12, sector II operation will have a voltage dip of less than 30 V and recovery time of 7 s. As expected, sector II has much better performance, as the stored kinetic energy helps to match the load power requirement in sector II.

Results in Table II show that the dc-link voltage can recover well with a dip of 130 V since relationship (6) is satisfied for the operating PMG speed and voltage range. When the PMG voltage approaches the rated value of 460 V, the voltage dip in Table II will be too large for the specified load change. A higher nominal dc-link voltage (e.g., 800 V) can be selected to have sufficient margin, which will be beneficial for stored capacitor energy as well.

B. Experimental Results

A 1-kW laboratory prototype PMG test bed was built, as shown in Fig. 13. It consists of a three-phase PMG, a generator-side converter to control the speed of the shaft, a dynamometer consisting of a three-phase induction motor driven by a commercial inverter, and a dc-link load resistor. The commercial inverter with torque control mode is used to emulate the wind power characteristics. The control board is based on a SHARC DSP AD21160M and Xilinx XCV-400 FPGA. The experimental parameters are shown in Table III. The compensated system has a bandwidth $f_0 = 0.01$ Hz to have a 70° phase margin. The corresponding proportional and integral gains for the PI regulator are 0.4 and 0.02, respectively. The dc-link voltage error threshold Δ for adaptive controller is chosen to be 10 V.

The control is tested with different load steps and emulated wind speed changes, similar to simulation cases conducted. The PMG in this case operates in sector I to test the more challenging scenarios. Fig. 14 shows selected steady-state waveforms of the experimental PMG and the converter. These waveforms validate the sensorless PMG control and the dc-link voltage regulation in steady state.

TABLE III
EXPERIMENTAL PARAMETERS

Rated Power	1 kW	Rated PMG Voltage	230 V
Rated PMG Current	3 A	Rated PMG Speed	157 rad/s
System Inertia	0.15 kgm^2	Rated VSC Dc-link Voltage	250 V
Rated Frequency f	60 Hz	VSC Dc-link Capacitance	2460 μF
D-axis Inductance L_d	21.5 mH	Q-axis Inductance L_q	19.5 mH
Stator Resistance R_s	3.5 Ω		

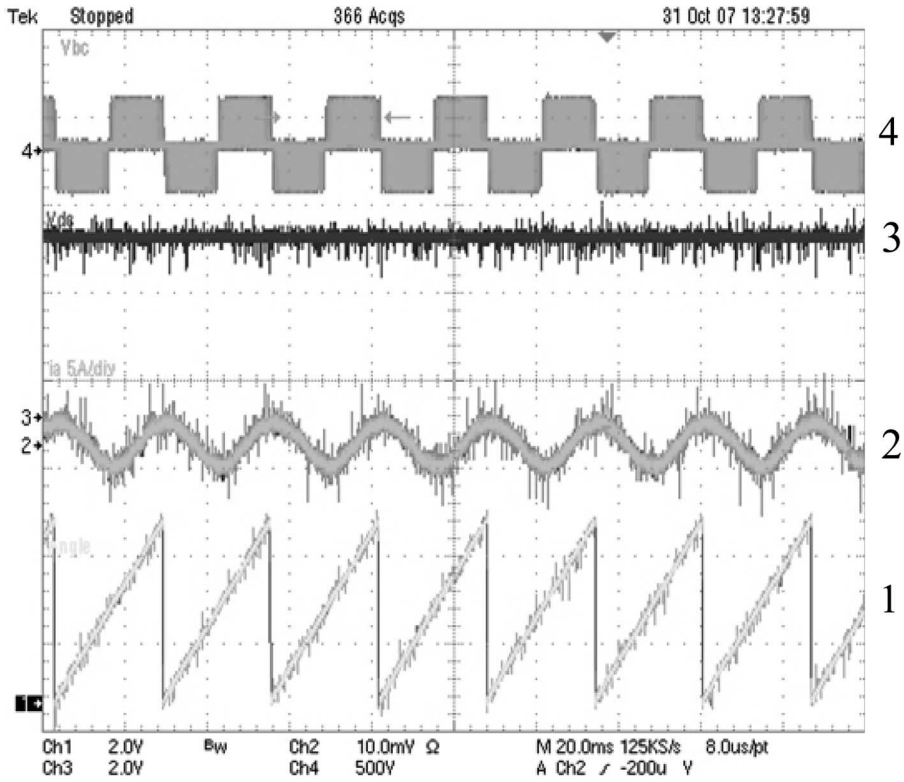

Fig. 14. Experimental steady-state waveforms: 1) estimated rotor position; 2) PMG current (5 A/division); 3) dc-link voltage (125 V/division); 4) PMG/converter line-to-line voltage V_{bc} (500 V/division).

Fig. 15 shows the measured waveforms for a load step from 180 to 250 W at $t = 40$ s: (a) the dc-link voltage dip and recovery and (b) the PMG output power measured by the DSP controller. As observed, the PMG output power shows a short decrease at the beginning of the transient due to the RHZ. Fig. 15(c) shows the speed reference and the matching estimated actual speed. Fig. 16 shows dc-link voltage response to the wind speed increase, emulated by 200 W increase in the dynomometer driving power at time $t = 25$ s, and the voltage is controlled back to the nominal 250 V. Note that, in order to shorten the dc-link voltage recovery time, a larger step change of the adaptive controller proportional gain was used for the experimental setup ($\Delta K_p = 0.08$ in experiment versus $\Delta K_p = 0.01$ in simulation). The higher gain introduced some oscillations to the dc-link voltage, as observed in Fig. 15, which are not present in simulation. In addition, considering the DSP computation capability limitations, the adaptive controller control cycle was set ten times longer than in the simulation, which also negatively affected the system performance.

Fig. 17 shows as a comparison of the system response using the simple PI voltage regulator under the same load step condition, as in Fig. 15. Fig. 17(a) shows that the voltage dip is similar to that of Fig. 15(a) but with longer recovery time. If the PI regulator bandwidth is increased, the recovery time will be reduced but the voltage variation will be worse and even start to oscillate, as shown in Fig. 17(b). The adaptive controller does lead to better overall performance.

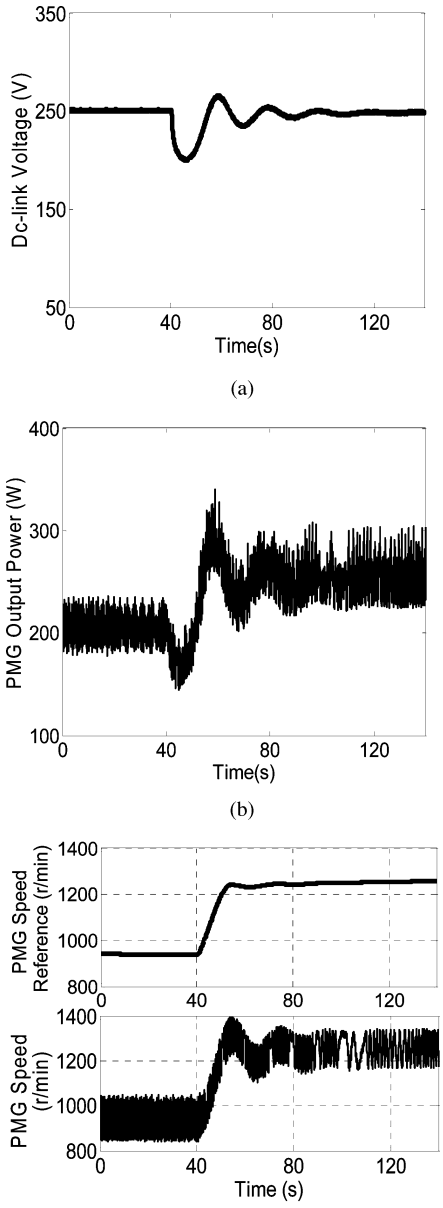

Fig. 15. Experimental waveforms during a load step change using the adaptive control. (a) DC-link voltage. (b) PMG output power. (c) PMG reference and actual speed.

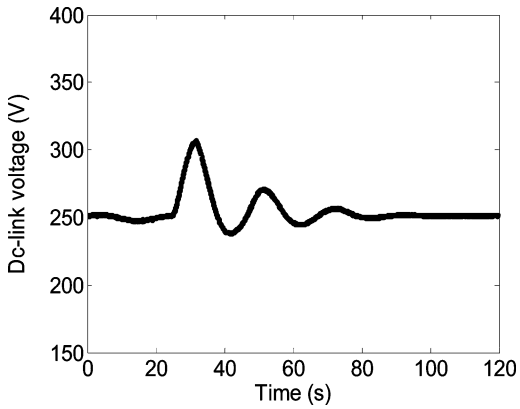

Fig. 16. DC-link voltage response with emulated wind speed increase.

IV. Discussions

A. Wind Speed Change

Most analysis so far assumed a constant wind speed. As wind speed changes, the controller should adjust the PMG operating point to maintain the dc-link voltage. For given load power, there are two possible scenarios when wind speed changes: 1) the operating point remains in the same sector and 2) the operating point switches from one sector to the other, which can occur for a fast wind speed change.

The first scenario is illustrated in Fig. 18(a). Initially, the wind generator is working at point A in sector I with load power 600 kW and wind speed 12 m/s. Suddenly, the wind speed reduces from 12 to 10 m/s and the operating point changes to B, and then controlled to point C, all in sector I. For the second scenario in Fig. 18(b), the wind speed increases from 10 to 12 m/s, causing the operating point A to change to point B (from sector II to sector I), and the PMG should be controlled to operating point C in sector I. Using the dc-link controller setting described in Section III, Fig. 19 shows the simulation results corresponding to the two scenarios in Fig. 18.

B. Transition Between MPPT and Weak-Grid Modes

The grid-side converter is generally responsible for the detection of strong or weak-grid conditions. Once the grid mode is known, it is convenient to transition from strong-grid (MPPT) mode to weak-grid mode and *vice versa*. With the proposed weak-grid mode dc-link voltage controller, the MPPT mode can be simply achieved by setting the dc-link voltage reference high and out of the real dc-link voltage range without changing the controller structure. The saturated voltage and speed regulators will command the system to generate as much power as possible, transitioning to MPPT mode automatically. On the other hand, when the weak-grid condition occurs, the dc-link voltage reference will be reset to the nominal value, thus regulating the excessive power from the MPPT mode down to match the load need. Fig. 20 illustrates a weak grid to MPPT mode transition process and the corresponding simulation of the sample system in Table I under a given wind speed. Note that the antiwindup and initial reference values must be properly set for the voltage and speed regulators during the mode transition for proper operations.

C. Pitch Angle Control

The study so far assumes a fixed pitch angle of 0° for simplicity. In large variable-speed wind turbines, where active pitch control is available, it can be used to adjust the captured wind power, together with PMG speed control. It has been shown in [31] that even with a maximum pitching rate of 10°/s, the pitch control cannot significantly mitigate the dc-link voltage variation. Therefore, the pitch angle control may work together with the speed regulator as part of the dc-link voltage controller proposed in this paper.

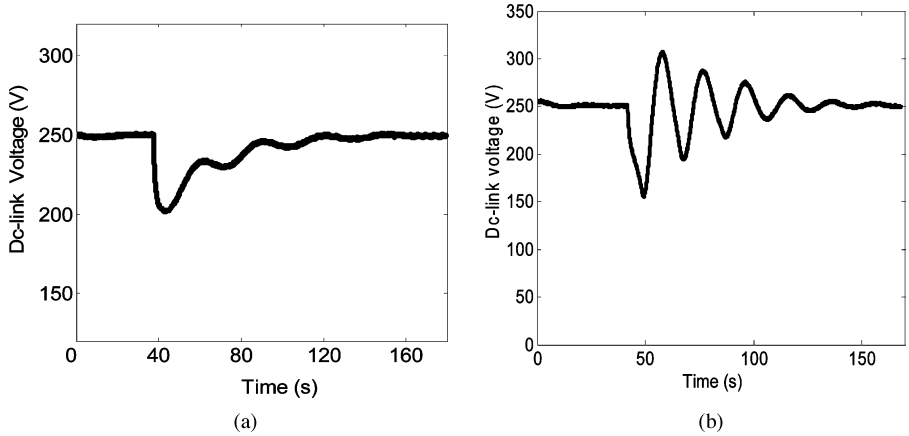

(a) (b)

Fig. 17. DC-link voltage during a load step using the simple PI control. (a) Original PI regulator. (b) Higher bandwidth PI regulator.

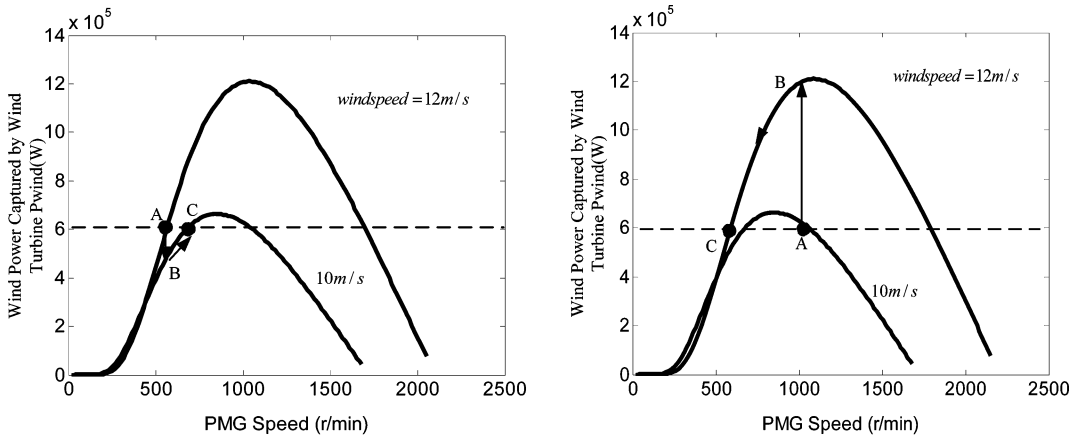

(a) (b)

Fig. 18. Operating point change during wind speed change. (a) Wind speed decrease, all points in sector I. (b) Wind speed increase, operation switch from sector II to sector I.

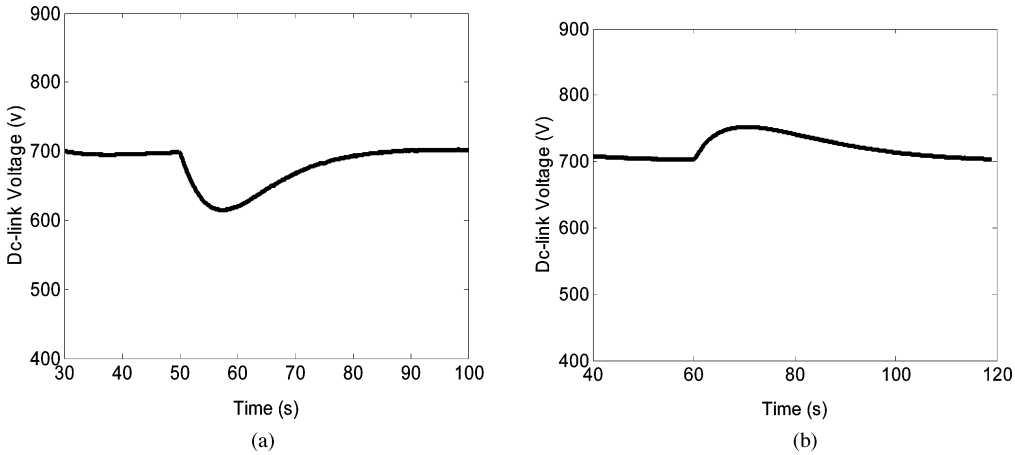

(a) (b)

Fig. 19. DC-link voltage simulation results during sudden wind speed change. (a) Scenario I. (b) Scenario II.

D. DC-Link Voltage Range

The dc-link voltage must be controlled within a range for the system to work properly. The minimum value of the dc-link voltage should meet the grid-side ac voltage amplitude requirement, and the maximum value should not exceed the voltage ratings of the converter components. In the example system studied with wind generation characteristics of Fig. 3, the dc-link voltage range used was chosen between 650 and 800 V, corresponding to the 460 V ac grid, with power level 1.5 MW, generator speed range 0–2400 r/min, and wind speed ranging from

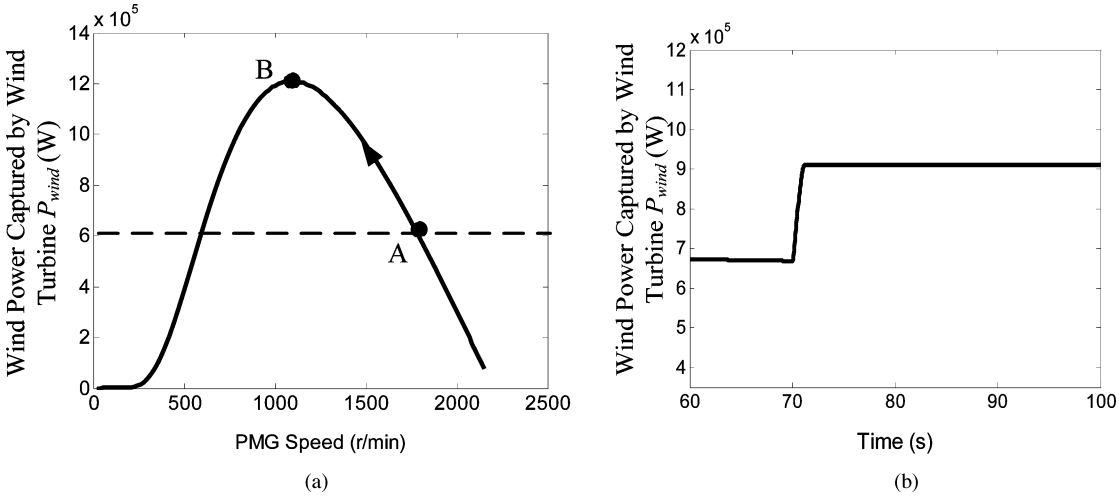

Fig. 20. Transition from the weak-grid mode to MPPT mode. (a) Operating point change. (b) Simulation of P_{wind} change.

3.5 m/s (cut-in wind speed) to 25 m/s (cutout wind speed). Note that although the voltage control design and performance will be affected by these system parameters, as well as by converter ratings, and dc-link energy storage and load characteristics, the methodology proposed in this paper allows for considering their impact on control design to achieve the desired performance.

When the PMG operates in weak-grid mode, sudden load power decrease or source increase will cause dc-link voltage rise. The proposed control with proper dc-link energy storage will help to reduce the voltage rise. However, itwould still be a good practice to use some protection methods to avoid damaging overvoltage conditions. These methods include those used already in wind applications, such as the dc-link crowbar circuit and turning off PMG-side converter switches [e.g., insulated gate bipolar transistors (IGBTs)] to limit the voltage. The protection will help to limit excessive energy storage requirement in extreme cases.

V. Conclusion

This paper has shown that to meet the need of operating a PMG-based wind power system in a weak grid, it is feasible to regulate the dc-link voltage of the full power VSC, with the generator-side converter controlling the PMG speed. The effectiveness of the control, measured by how fast the captured wind power can be adjusted through the PMG speed control to match the load power variation, depends primarily on the characteristics of wind power versus turbine/generator speed, the system mechanical inertia, as well as the dc-link capacitor. While the capacitor always helps, the system inertia can slow down the control if the wind generator operates on the part of the wind power–speed curves with positive slopes, where there also exists an intrinsic RHZ further limiting the system response. For best dc-link voltage regulation during a load change, the PMG output power change rate should be maximized by searching for a corresponding optimal PMG speed change rate dynamically. The proposed control algorithm in this paper can achieve the optimal $d\omega/dt$ search through adapting the proportional gain of a PI regulator. The algorithm has been implemented and verified in both simulation and experiment. Due to the large mechanical inertia in a wind system, sufficiently large dc-link energy storage is needed to handle the transient load variations. Even with the conventional capacitors, the size of the required energy storage is acceptable and can be further reduced with other advanced technologies. The proposed control method in the weak-grid mode can perform well with changing wind speeds, can be combined with turbine pitch angle control, and can also transition seamlessly to and from the MPPT mode.

References

[1] Q. Wang and L. Chang, "An intelligent maximum power extraction algorithm for inverter-based variable speed wind turbine systems," *IEEE Trans. Power Electron.*, vol. 19, no. 5, pp. 1242–1249, Sep. 2004.

[2] F. Blaabjerg and Z. Chen, *Power Electronics for Modern Wind Turbines*. San Rafael, CA: Morgan & Claypool, 2006, ch. 4.

[3] Z. Lubosny, *Wind Turbine Operation in Electric Power Systems*. Berlin, Germany: Springer-Verlag, 2003, ch. 1.

[4] I. Erlich and F. Shewarega, "Interaction of large wind power generation plants with the power system," in *Proc. IEEE PECon 2006 Conf.*, Nov., vol. 1, pp. 12–18.

[5] S. Grabic, N. Celanovic, and V. A. Katic, "Permanent magnet synchronous generator cascade for wind turbine application," *IEEE Trans. Power Electron.*, vol. 23, no. 3, pp. 1136–1142, May 2008.

[6] J. M. Carrasco, E. Galvan, R. Portillo, and L. G. Franquelo, "Power electronic systems for grid integration of wind turbines," in *Proc. IEEE IECON 2006 Conf.*, Nov., pp. 4182–4188.

[7] X. Zeng, Z. Chen, and F. Blaabjerg, "Design and comparison of full-size converters for large variable-speed wind turbines," in *Proc. EPE 2007 Conf.*, Sep., vol. 1, pp. 1–10.

[8] C. Ng, M. Parker, and P. Tavner, "A multilevel modular converter for a large light weight wind turbine generator," *IEEE Trans. Power Electron.*, vol. 23, no. 3, pp. 1062–1074, May 2008.

[9] M. Chinchilla, S. Arnaltes, and J. Burgos, "Control of permanent-magnet generators applied to variable-speed wind-energy systems connected to the grid," *IEEE Trans. Energy Convers.*, vol. 21, no. 1, pp. 130–135, Mar. 2006.

[10] J. A. Baroudi, V. Dinavahi, and A. M. Knight, "A review of power converter topologies for wind generators," in *Proc. IEEE Electr. Mach. Drives Int. Conf.*, May 2005, vol. 1, pp. 458–465.

[11] R. C. Portillo, M. Angeles, and M. Prats, "Modeling strategy for back-to-back three-level converters applied to high-power wind turbines," *IEEE Trans. Ind. Electron.*, vol. 53, no. 5, pp. 1483–1491, Oct. 2006.

[12] K. Tan and S. Islam, "Optimum control strategies in energy conversion of PMSG wind turbine system without mechanical sensors," *IEEE Trans. Energy Convers.*, vol. 19, no. 2, pp. 392–399, Jun. 2004.

[13] T. Ahmed, K. Nishida, and M. Nakaoka, "Advanced control of PWM converter with variable-speed induction generator," *IEEE Trans. Ind. Appl.*, vol. 42, no. 4, pp. 934–945, Jul./Aug. 2006.
[14] E. Hau, *Wind-Turbines Fundamentals, Technologies, Application, Economics*. Berlin, Germany: Springer-Verlag, 2000, ch. 8–10.
[15] F. Blaabjerg, Z. Chen, and S. B. Kjaer, "Power electronics as efficient interface in dispersed power generation systems," *IEEE Trans. Power Electron.*, vol. 19, no. 5, pp. 1184–1194, Sep. 2004.
[16] T. Sun, Z. Chen, and F. Blaabjerg, "Voltage recovery of grid-connected wind turbine after a short-circuit fault," in *Proc. IEEE IECON 2003*, Nov., vol. 3, pp. 2723–2728.
[17] E. Koutroulis and K. Kalaitzakis, "Design of a maximum power tracking system for wind-energy-conversion applications," *IEEE Trans. Ind. Electron.*, vol. 53, no. 2, pp. 486–494, Apr. 2006.
[18] R. Spee, S. Bhowmik, and J. Enslin, "Novel control strategies for variable speed doubly fed wind power generation systems," *Renew. Energy*, vol. 6, pp. 907–915, Nov. 1995.
[19] A. Z. Mohamed, M. N. Eskander, and F. A. Ghali, "Fuzzy logic control based maximum power tracking of a wind energy system," *Renew. Energy*, vol. 23, pp. 235–245, Jun. 2001.
[20] R. Esmaili, L. Xu, and D. K. Nichols, "A new control method of permanent magnet generator for maximum power tracking in wind power tracking in wind turbine application," in *Proc. IEEE PES 2005 Gen. Meeting*, Jun., vol. 3, pp. 2090–2095.
[21] R. Tirumala, N. Mohan, and C. Henze, "Seamless transfer of grid connected PWM inverters between utility-interactive and Stand-alone modes," in *Proc. IEEE APEC 2002 Conf.*, Mar., vol. 2, pp. 1081–1086.
[22] R. Teodorescu and F. Blaabjerg, "Flexible control of small wind turbines with grid failure detection operating in stand-alone and grid-connected mode," *IEEE Trans. Power Electron.*, vol. 19, no. 5, pp. 1323–1332, Sep. 2004.
[23] A. Binder and T. Schneider, "Permanent magnet synchronous generators for regenerative energy conversion—A survey," in *Proc. EPE 2005 Conf.*, Sep., vol. 1, pp. 10–15.
[24] E. Muljadi, S. Drouilhet, R. Holz, and V. Gevorgian, "Analysis of permanent magnet generator for wind power battery charging," in *Proc. IEEE IAS 1996 Conf.*, Oct., vol. 1, pp. 541–548.
[25] L. Ran, J. R. Bumby, and P. J. Tavner, "Use of turbine inertia for power smoothing of wind turbines with a DFIG," in *Proc. Harmonics Qual. Power Conf.*, Sep. 2004, vol. 1, pp. 106–111.
[26] A. Mullane, G. Bryans, and M. O'Malley, "Kinetic energy and frequency response comparisons for renewable generation systems," in *Proc. Future Power Syst. Conf.*, Nov. 2005, vol. 1, pp. 16–18
[27] S. Morimoto, Y. Taked, and T. Hirasa, "Current phase control method for permanent magnet synchronous motors," *IEEE Trans. Power Electron.*, vol. 5, no. 2, pp. 133–139, Apr. 1990.
[28] R. P. Burgos, P. Kshirsagar, and A. Lidozzi, "Design and evaluation of a PLL-based position controller for sensorless vector control of permanent-magnet synchronous machines," in *Proc. IEEE IECON 2006 Conf.*, Nov., vol. 2, pp. 5081–5086.
[29] S. Bolognani, M. Tomasini, and L. Tubiana, "Start-up strategy for a sensorless direct drive PM generator for wind turbines," in *Proc. ISIE 2005 Conf.*, Sep., vol. 2, pp. 1081–1086.
[30] Z. Wang and L. Chang, "A DC voltage monitoring and control method for three-phase grid-connected wind turbine inverters," *IEEE Trans. Power Electron.*, vol. 23, no. 3, pp. 1118–1125, May 2008.
[31] J. F. Conroy and R. Watson, "Low-voltage ride-through of a full converter wind turbine with permanent magnet generator," *IET Renew. Power Gener.*, vol. 1, no. 3, pp. 182–189, May 2007.

Xibo Yuan (S'09) received the B.S. degree in electrical engineering from China University of Mining and Technology, Xuzhou, China, in 2005. He is currently working toward the Ph.D. degree in electrical engineering at Tsinghua University, Beijing, China.

From 2007 to 2008, he was a Visiting Scholar with the Center for Power Electronics Systems (CPES), Virginia Polytechnic Institute and State University, Blacksburg. His current research interests include wind power generation, control of multilevel converters, and sensorless drive of induction motor and permanent-magnet motor.

Fei (Fred) Wang (S'87–M'91–SM'99) received the B.S. degree from Xi'an Jiaotong University, Xi'an, China, and the M.S. and Ph.D. degrees from the University of Southern California, Los Angeles, in 1982, 1985, and 1990, respectively, all in electrical engineering.

From 1990 to 1992, he was a Research Scientist with the Electric Power Laboratory, University of Southern California. In 1992, he joined the GE Power Systems Engineering Department, Schenectady, NY, as an Application Engineer. From 1994 to 2000, he was a Senior Product Development Engineer with GE Industrial Systems, Salem, VA. During 2000–2001, he was the Manager of Electronic and Photonic Systems Technology Laboratory, GE Global Research Center, Schenectady, NY, and Shanghai, China. In 2001, he joined the Center for Power Electronics Systems (CPES), Virginia Polytechnic Institute and State University (Virginia Tech), Blacksburg, where he is currently the Technical Director and an Associate Professor. His research interests include power electronics, power systems, controls, electric machines, and motor drives.

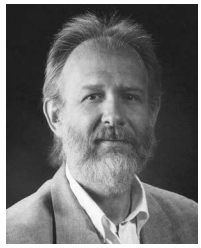

Dushan Boroyevich (S'83–M'85–SM'03–F'06) received the Dipl. Ing. degree from the University of Belgrade, Belgrade, Serbia, in 1976, the M.S. degree from the University of Novi Sad, Novi Sad, Serbia, in 1982, and the Ph.D. degree from Virginia Polytechnic Institute and State University (Virginia Tech), Blacksburg, in 1986.

From 1986 to 1990, he was an Assistant Professor and the Director of the Power and Industrial Electronics Research Program, Institute for Power and Electronic Engineering, University of Novi Sad, where he later became the Head. He then joined the Bradley Department of Electrical and Computer Engineering, Virginia Tech, as an Associate Professor, where he is currently the American Electric Power Professor and the Co-Director of the National Science Foundation (NSF) Engineering Research Center for Power Electronics Systems (CPES). His research interests include multiphase power conversion, electronic power distribution systems, power electronics systems modeling and control, and multidisciplinary design optimization.

Prof. Boroyevich is a recipient of the IEEE William E. Newell Power Electronics Technical Field Award.

Yongdong Li (M'08) was born in Hebei, China. He received the B.S.E.E. degree from Harbin Institute of Technology, Harbin, China, in 1982, and the M.S.E.E. and Ph.D. degrees from the Department of Electrical Engineering, Institute National Polytechnique de Toulouse, Toulouse, France, in 1984 and 1987, respectively.

From 1988 to 1990, he was a Postdoctoral Researcher from 1988 to 1990 with the Department of Electrical Engineering, Tsinghua University, where he was an Associate Professor from 1991 to 1996, has been a Professor since 1996, and is also with the Laboratory of Power Electronics and Motor Control. During 1995, he was a Visiting Scholar with the Department of Electrical Engineering, Yokohama National University, Japan. From June to December 1996, he was a Visiting Professor with Virginia Power Electronics Center (VPEC), Virginia Polytechnique Institute and State University. During 2002, he was an Invited Professor of the Institute National Polytechnique de Toulouse, France. His research interests include control theories, real-time implementation, sensorless drives and applications of vector and direct torque control of ac motors, wind power generation, medium-voltage high-power inverter for motor drives, and active power filter application. He has authored or coauthored more than 200 conference and journal papers, and two monographs on digital control of ac motor and multilevel converter.

Prof. Li is a Senior Member of the China Electro-Technique Society, the Vice Chairman of the China Power Electronics Society, the Vice Chairman of the Electrical Automation Committee of China Automation Association.

Rolando Burgos (S'96–M'03) received the B.S. degree in electronics engineering, the Electronics Engineering Professional Degree, and the M.S. and Ph.D. degrees in electrical engineering from the University of Concepción, Concepción, Chile, in 1995, 1997, 1999, and 2002 respectively.

In 2002, he joined the Center for Power Electronics Systems (CPES), Virginia Polytechnic Institute and State University (Virginia Tech), Blacksburg, as a Postdoctoral Fellow, where he was a Research Scientist from 2003 to 2005, and a Research Assistant Professor at the Bradley Department of Electrical and Computer Engineering from 2005 to 2009. In 2009, he joined the ABB United States Corporate Research Center, Raleigh, NC, where he is currently a Power Electronics Consulting R&D Engineer. His research interests include multiphase power conversion, stability of ac and dc power electronics systems, hierarchical modeling, control theory, and the synthesis of power electronics conversion systems.

Dr. Burgos is a member of the IEEE Power Electronics Society, the IEEE Industrial Electronics Society, and the IEEE Industry Applications and Power Engineering Society, and is currently the Secretary of the Committee on Simulation, Modeling and Control of the Power Electronics Society.